

Fusion of Evidences in Intensities Channels for Edge Detection in PolSAR Images

Anderson Adaime de Borba - Mackenzie-BR - IBMEC-SP

Dr. Mauricio Marengoni - Mackenzie-BR

Dr. Alejandro Frery - UFAL-BR

August 24, 2020

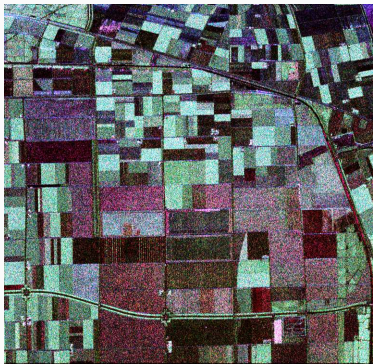
IBMEC-SP - 2020

PolSAR Image

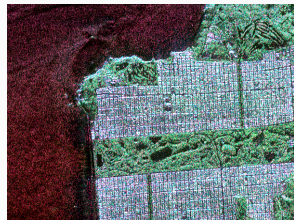
PolSAR important characteristics

- Can be on raised platforms, crewed aircraft or not, satellites orbiting the earth or other planets;
- It is a viable and practical imaging technique;
- PolSAR images has a high resolution;
- Synthesizes long antenna openings;
- Radars produce images day and night;
- Climate does not interfere in image capture;
- SAR imaging systems operate in the microwave region of the electromagnetic spectrum, usually between the P-band - and the K-band.

PolSAR Image



(a) Flevoland Image



(b) San Francisco Bay

Figure 1: PolSAR image example

Economy and Administration Applications

- EOxposure- Project with European Union ;

Economy Applications - The Gross Domestic Product - GDP

- Article address;

Economy and Administration Applications - The View from Above: Applications of Satellite Data in Economics

- Article address;

PolSAR Image

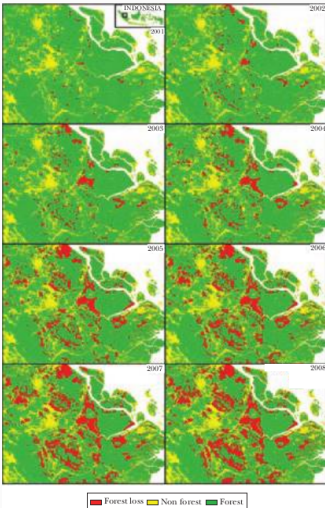


Figure 2: Forest Cover over Time in Riau Province, Ref. [1]

PolSAR Image

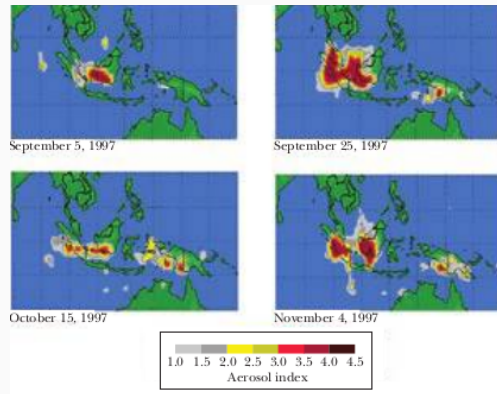


Figure 3: Aerosol Index of Particulate Air Pollution in Indonesia, Ref. [1]

PolSAR Image

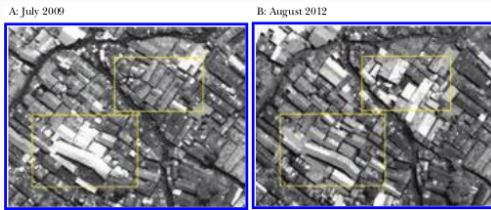


Figure 4: Roofs in Kibera, Nairobi, Ref. [1]

Economy and Administration Applications

- IBMEC QUANT CENTER;

Statistical modeling for PolSAR data (1 - Look)

- The complex scattering matrix \mathbf{S} :

$$\mathbf{S} = \begin{bmatrix} S_{hh} & S_{hv} \\ S_{vh} & S_{vv} \end{bmatrix}. \quad (1)$$

- The medium of propagation of waves is reciprocal

$$\mathbf{s} = [S_{hh}, S_{hv}, S_{vv}]^T.$$

Statistical modeling for PolSAR data (1 - Look)

- The probability density function (pdf):

$$f_s(s; \Sigma) = \frac{1}{\pi^3 |\Sigma|} \exp(-s^H \Sigma^{-1} s), \quad (2)$$

- $|\cdot|$ is the determinant,
- H denotes the conjugate complex number,
- Σ is the covariance matrix of s such that $\Sigma = E[ss^H]$,
- $E[\cdot]$ denotes the expected value.
- The distribution of s is assumed to be Gaussian circular complex multivariate with zero mean $N_3^C(0, \Sigma)$.

Statistical modeling for PolSAR data (L - Looks)

- The estimated sample covariance matrix:

$$\mathbf{Z} = \frac{1}{L} \sum_{\ell=1}^L \mathbf{s}_\ell \mathbf{s}_\ell^H, \quad (3)$$

- \mathbf{s}_ℓ , $\ell = 1, \dots, L$;
- L independent samples of complex vectors distributed as \mathbf{s} .

Statistical Modeling

Statistical modeling for PolSAR data (L - Looks)

- Multilooked Wishart distribution with probability density function:

$$f_{\mathbf{Z}}(\mathbf{Z}; \Sigma_s, L) = \frac{L^{mL} |\mathbf{Z}|^{L-m}}{|\Sigma_s|^L \Gamma_m(L)} \exp(-L \text{tr}(\Sigma_s^{-1} \mathbf{Z})), \quad (4)$$

- $\text{tr}(\cdot)$ is the trace operator,
- $\Gamma_m(L)$ is a multivariate Gamma function

$$\Gamma_m(L) = \pi^{\frac{1}{2}m(m-1)} \prod_{i=0}^{m-1} \Gamma(L-i),$$

- $\Gamma(\cdot)$ is the Gamma function,
- $m = 3$,
- $\mathbf{Z} \sim W(\Sigma, L)$,

Edges detection

Method

The following procedure is proposed to detected edges in the hh, hv and vv channels:

- identify the centroid of a region of interest (ROI) in an automatic, semi-automatic or manual manner;
- cast rays from the centroid to the outside of the area;
- collect data around the rays using the Bresenham's midpoint line algorithm, ideally the size of a pixel;
- detect points in the data strips which provide evidence of changes in their statistical properties, i.e., a transition point that defines edge evidence;
- use the Generalized Simulated Annealing (GenSA) method, Ref. [2], to find maximum points in the functions of interest;
- fuse the evidence of detected edges in the hh, hv and vv channels.

Edges detection

ROI Flevoland Example

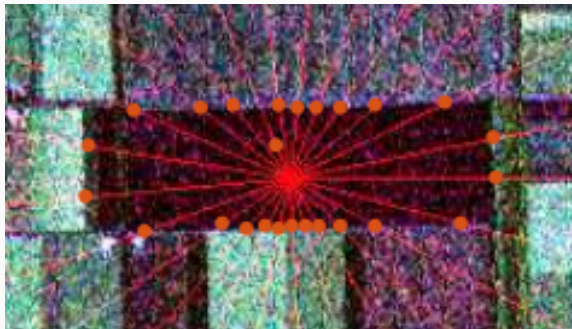


Figure 5: Edges detection example (hh channel).

Edges detection

Maximum Likelihood Estimator (MLE)

- Suppose $\mathbf{X} = (X_1, X_2, \dots, X_n)^T$ is a random vector distributed according to the probability density function $f(\mathbf{x}, \theta)$ with parameters $\theta = (\theta_1, \dots, \theta_d)^T$ in the parameter space Θ .
- The likelihood function is

$$L(\theta; \mathbf{X}) = \prod_{i=1}^n f(x_i; \theta),$$

- log-likelihood function is

$$\ell(\theta; \mathbf{X}) = \ln L(\theta; \mathbf{X}) = \sum_{i=1}^n \ln f(x_i; \theta), \quad (5)$$

- $\hat{\theta} = \arg \max_{\theta \in \Theta} L(\theta; \mathbf{x}),$
- $\hat{\theta} = \arg \max_{\theta \in \Theta} \ell(\theta; \mathbf{x}).$

Edges detection

Maximum Likelihood Estimator (MLE)

$$\ell(L, \mu; z) = n[L \ln(L/\mu) - \ln \Gamma(L)] + L \sum_{k=1}^n \ln z_k - \frac{L}{\mu} \sum_{k=1}^n z_k. \quad (6)$$

Applied to the sample $z = (z_1, z_2, \dots, z_n)$,

$$z = (\underbrace{z_1, z_2, \dots, z_j}_{z_l}, \underbrace{z_{j+1}, z_{j+2}, \dots, z_n}_{z_E}).$$

Edges detection

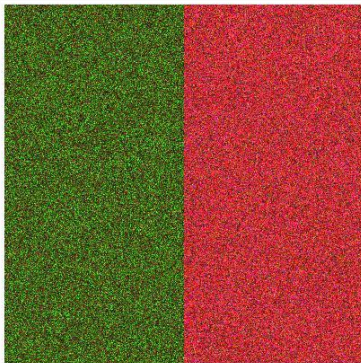
Maximum Likelihood Estimator (MLE)

We then compute the total log-likelihood of z_I and z_E :

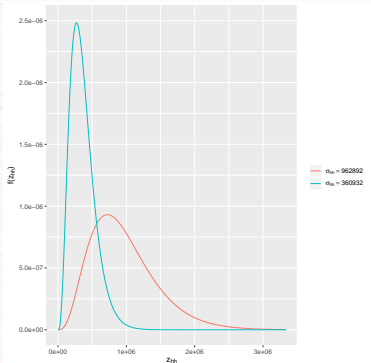
$$\begin{aligned}\ell_T(j; \hat{\mu}_I, \hat{L}_I, \hat{\mu}_E, \hat{L}_E) = & - \left(\frac{\hat{L}_I}{\hat{\mu}_I} \sum_{k=1}^j z_k + \frac{\hat{L}_E}{\hat{\mu}_E} \sum_{k=j+1}^n z_k \right) + \\ & j [\hat{L}_I \ln(\hat{L}_I/\hat{\mu}_I) - \ln \Gamma(\hat{L}_I)] + \hat{L}_I \sum_{k=1}^j \ln z_k + \\ & (n-j) [\hat{L}_E \ln(\hat{L}_E/\hat{\mu}_E) - \ln \Gamma(\hat{L}_E)] + \hat{L}_E \sum_{k=j+1}^n \ln z_k.\end{aligned}\tag{7}$$

Edges detection

Application in simulated images



(a) Pauli decomposition



(b) Marginal densities of the hh channel

Figure 6: Model and observations

Edges detection

Application in simulated images

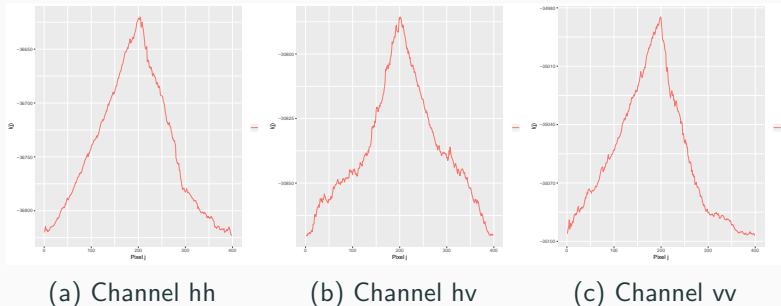


Figure 7: $I(j)$ log-likelihood function

Edges detection

Application in simulated images

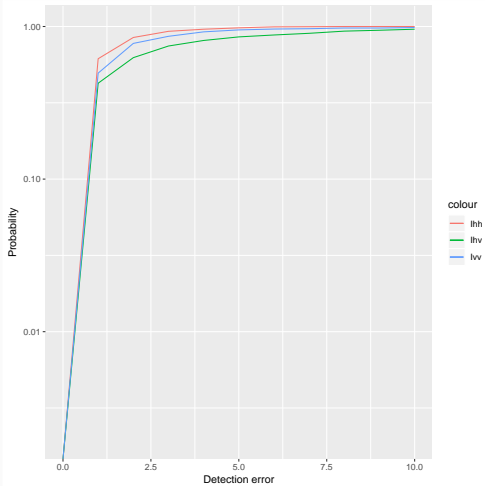


Figure 8: Probability of detecting edges evidences.

Evidence Fusion

Average Fusion

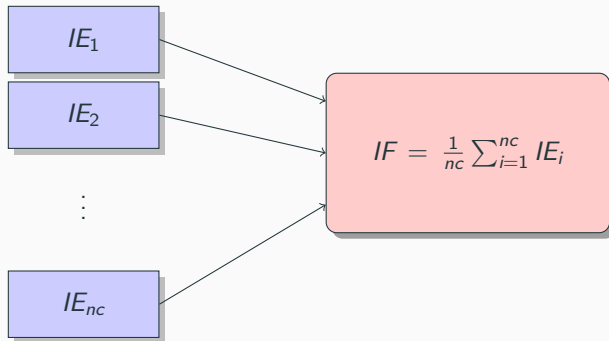


Figure 9: Average Fusion.

Evidence Fusion

PCA Fusion

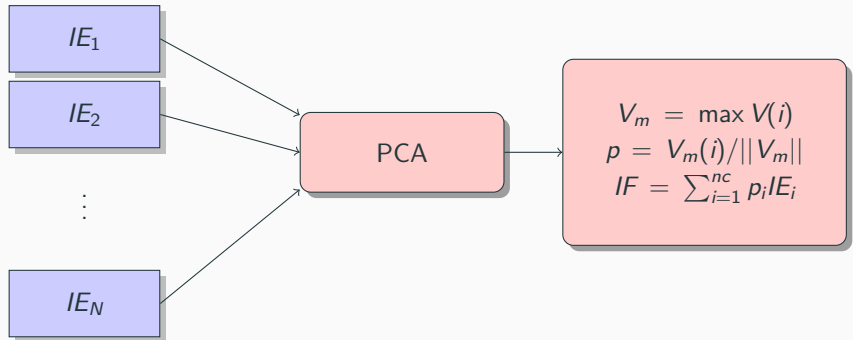


Figure 10: PCA Fusion.

Evidence Fusion

Stationary wavelet transform – SWT Fusion

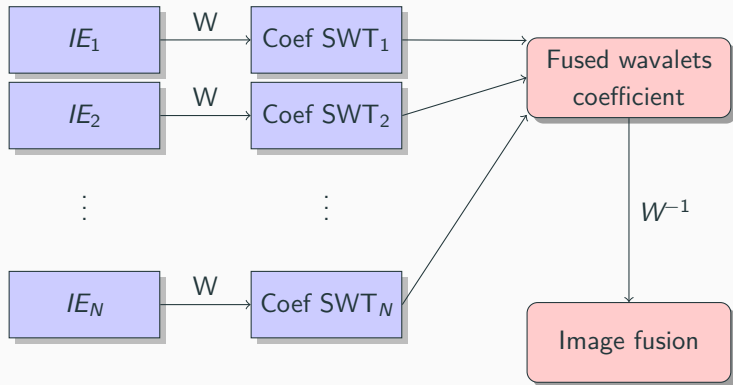


Figure 11: SWT Fusion.

- W is wavelet transformed.

Conclusion

Discrete wavelet transform – DWT Fusion

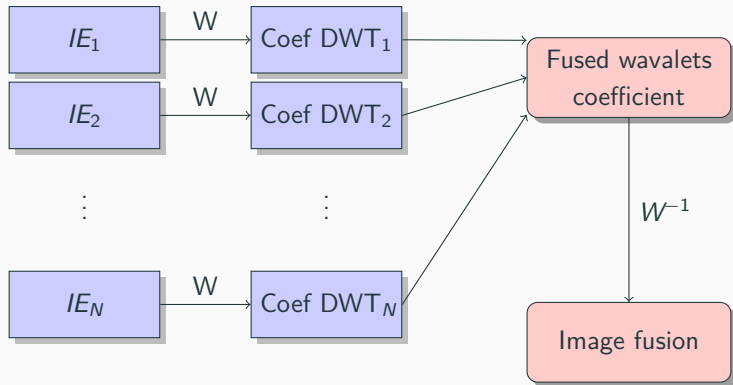


Figure 12: DWT Fusion.

Evidence Fusion

ROC statistics Fusion

- Part I

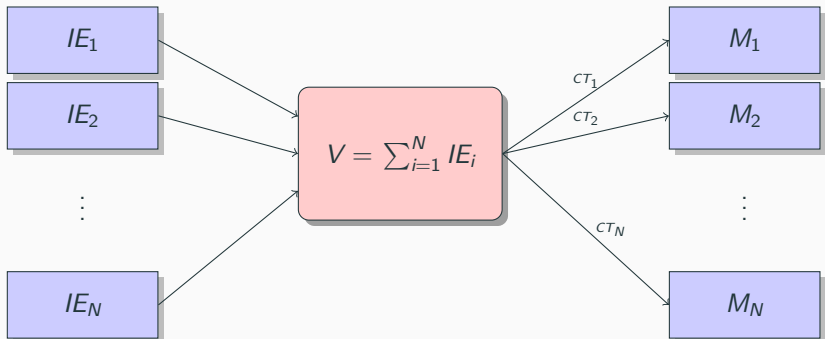


Figure 13: Fusion based in ROC statistics - Part I.

- CT_i is a threshold.

Evidence Fusion

ROC statistics Fusion

- Part II - for each M_j

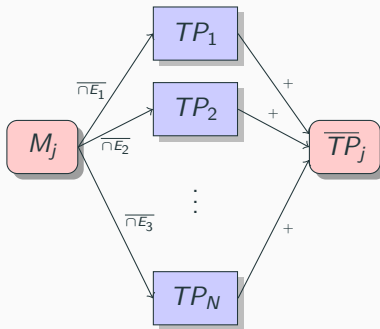


Figure 14: ROC Fusion for each j . It is true to \overline{TN}_j , \overline{FP}_j and, \overline{FN}_j .

- To generate the confusion matrix, and calculate the ROC statistics.

Results

Results

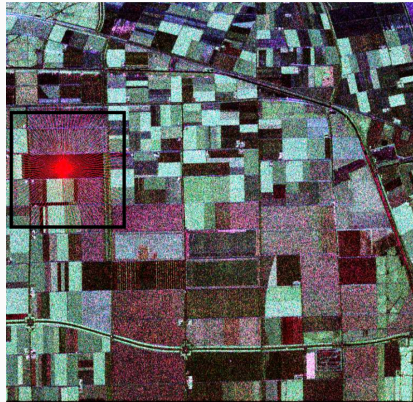
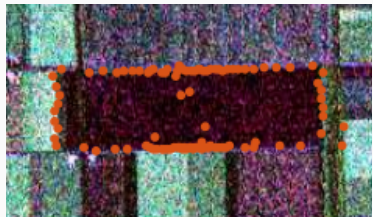


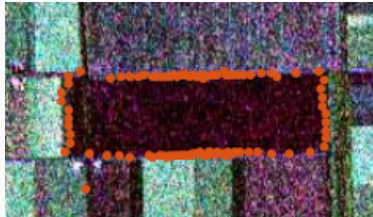
Figure 15: Region of interest (ROI) in the image of Flevoland.

Results

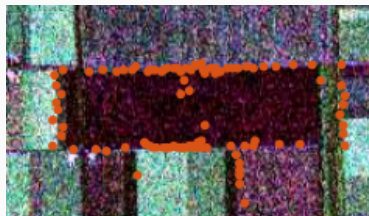
Results



(a) Evidences in channel hh



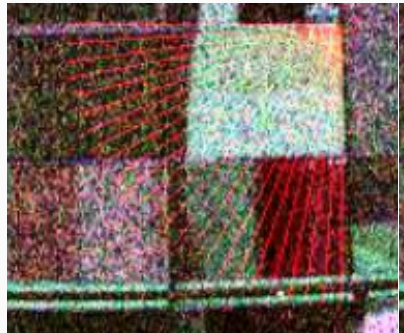
(b) Evidences in channel hv



(c) Evidences in channel vv

Results

Results



(a) Image and rays.



(b) Ground reference

Figure 17: Flevoland image in Pauli decomposition, and ground reference

Results

Results

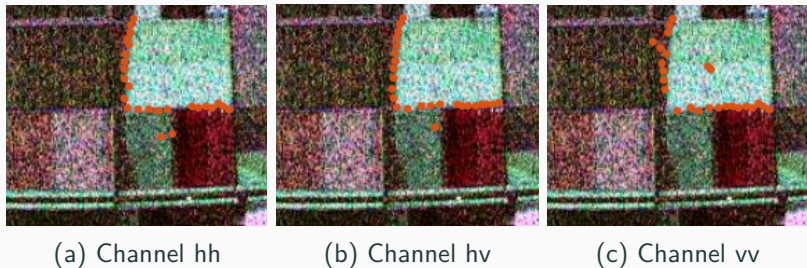
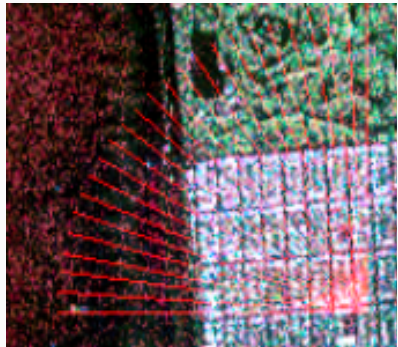


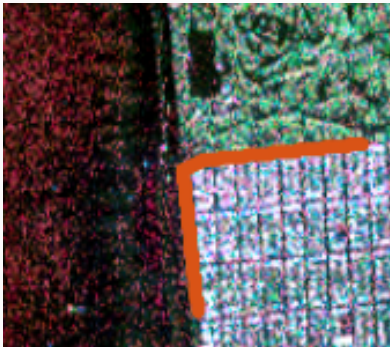
Figure 18: Edges evidences from the three intensity channels, Flevoland image

Results

Results



(a) Image and rays.



(b) Ground reference

Figure 19: San Francisco image in Pauli decomposition, and ground reference

Results

Results

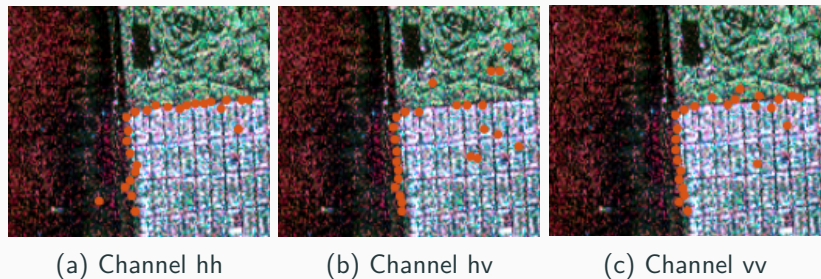
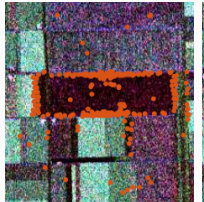


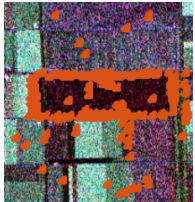
Figure 20: Edges evidences from the three intensity channels to San Francisco

Results- Fusion

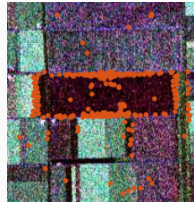
Results



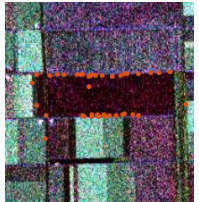
(a) Average



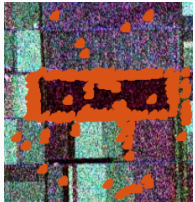
(b) MR-DWT



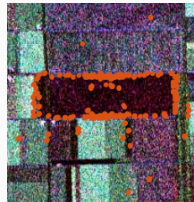
(c) PCA



(d) ROC



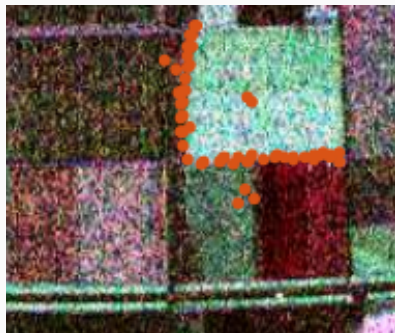
(e) MR-SWT



(f) MR-SVD

Results - Fusion

Results



(a) PCA fusion

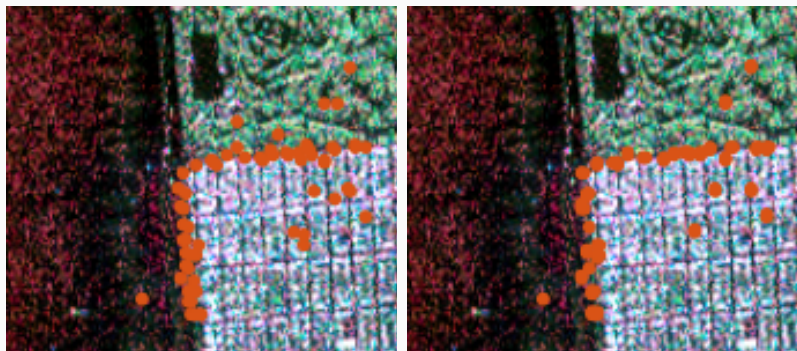


(b) MR-SVD fusion

Figure 22: Two best fusion results in the Flevoland image

Results - Fusion

Results



(a) PCA fusion

(b) MR-SVD fusion

Figure 23: Two best fusion results in the San Francisco image

Results - Fusion

Results

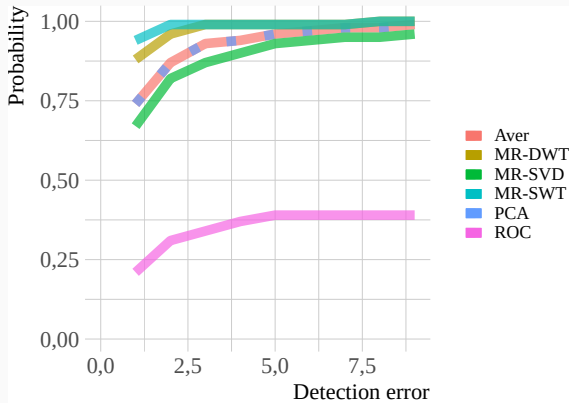


Figure 24: Probability of detecting the edge by the fusion methods.

Results - Fusion

Run time

Table 1: Processing times (fusion method).

Method	Aver.	PCA	MR-DWT	MR-SWT	ROC	MR-SVD
Time (s)	0.01	0.02	0.08	0.18	0.40	1.11
Rel. time	1.00	2.19	9.25	21.05	46.59	129.57

Conclusion

Conclusion

- Simulated Annealing works very well in non differentiable function.
- The fusion of evidence in intensity channels shows that these channels can be complementary and, therefore, suitable for edge detection in PolSAR images.
- The article shows the viability of these methods and your extension to more channels.
- The methods SVD fusion and PCA fusion have better performance taking into account accurate detection, run time and, the presence of outliers.

Future researches

- Increase the number of channels to improve the fusion;
- Investigate new fusion methods.

- ❑ D. Donaldson and A. Storeygard, “The View from Above: Applications of Satellite Data in Economics,” *Journal of Economic Perspectives*, vol. 30, no. 4, pp. 171–198, Fall 2016. [Online]. Available:
<https://ideas.repec.org/a/aea/jecper/v30y2016i4p171-98.html>
- ❑ Y. Xiang, S. Gubian, B. Suomela, and J. Hoeng, “Generalized Simulated Annealing for Global Optimization: The GenSA Package,” *The R Journal*, vol. 5, no. 1, pp. 13–28, 2013.